CHAPTER 2

PRINCIPLE AND THEORY

2.1 The Sun

The sun has temperature about 5777 K. The temperature at the central interior regions is estimated at 8×10^6 to 40×10^6 K. The temperature of many millions of degrees is transferred to the solar sphere surface and then is radiated into space. The sun radiation is in the x-ray and gamma-ray of the spectrum, with the wavelengths of the radiation increased by increasing the radial distances but the temperature decrease. It is estimated that 90% of the energy is produced at 0 to 0.23R (where R is the radius of the sun). The convection processes are beginning to important at a distance 0.7R from the center, and at from 0 to 1.0R is the convective zone.

2.1.1 The solar constant

Figure 2.1 shows schematically the sun-earth relationships. The eccentricity of the earth's orbit around the sun is 1.7%. 1.495×10^{11}m is the mean earth-sun distance. The *Gsc* is the constant of solar energy on a unit area of a surface perpendicular. Solar radiation measurements are *Gsc* = 1,367 W/m^2 (Duncan et al., 1981).

2.1.2 Types of solar radiation

The total solar radiation, often called as global radiation is the sum of direct, diffuse and reflected radiation shown in Figure 2.2. The solar radiation available to us is always a mix of the above mentioned three components (Aeron, 2015).

- Beam radiation**,** the solar radiation from the sun is not scattered by the atmosphere.

- Diffuse radiation, the solar radiation from the sun after its direction changes by scattering in the atmosphere.

- Total solar radiation**,** the sum of the beam and the diffuse solar radiation on a surface. The solar radiation measurements of total radiation on a horizontal surface which represent to as global radiation on the surface.

- Irradiance (W/m^2), the rate of radiant energy is incident on a surface per unit area of a surface. The symbol I_G is used for solar intensity.

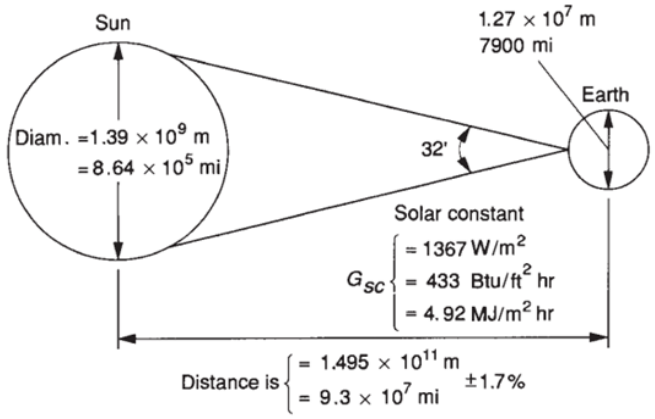

Figure 2.1 Sun-earth relationships (Iqbal, 1983)

2.1.3 Direction of beam radiation

The relationships of the incoming beam solar radiation on the earth can be explained of several angles. The angles and a set of consistent sign conventions are as follows (Benford & Bock, 1939) :

- Latitude (φ), the angular location north or south of the equator, north positive; $-90^\circ \leq \varphi \leq 90^\circ$.
- Declination (δ), the angular position of the sun at solar noon with respect to the plane of the equator, north positive; $-23.45^\circ \leq \delta \leq 23.45^\circ$.
- Slope (β), the angle between the plane of the surface in question and the horizontal; $0^\circ \leq \beta \leq 180^\circ$

2.1.4 Angle for tracking surfaces

Some solar collectors ‘‘track’’ the sun by moving in prescribed ways to decrease the incidence angle of solar radiation on their surfaces and thus maximize the incident solar radiation. The incidence angles and the surface angles are necessary for

these collectors (Marion & Urban, 1995), which in practice is usually horizontal north-south or parallel to the earth's axis shown in Figure 2.3. Thailand, a country bedstead in the southeastern part of Asia between 15°00' North latitude and 100°00' East longitude. Therefore, the solar water heater has the solar angle between 5-20 degrees to the horizontal panel, and the collector facing south because solar radiation is incident on collector all day.

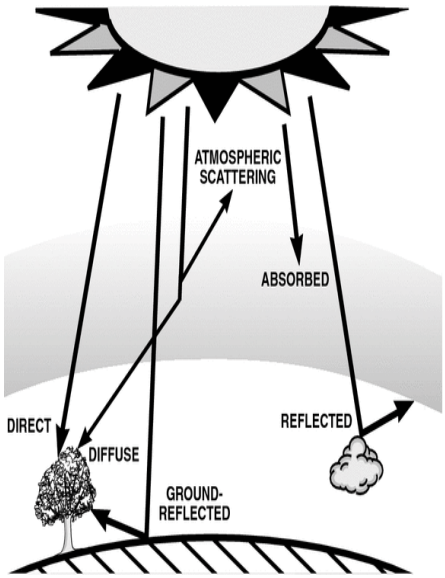

Figure 2.2 Some of the solar radiation entering the earth
(source: http://www.windows2universe.org)

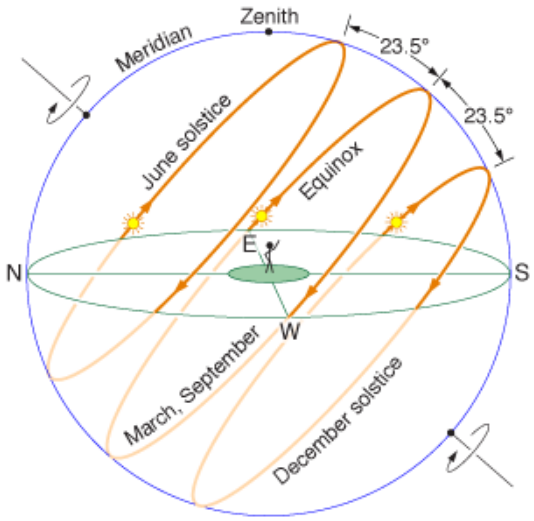

Figure 2.3 The Sky dome showing the sun angles for the solstices and equinox
(source: http://tboake.com/carbon-aia/strategies1a.html)

2.2 Solar collectors

Solar collectors are a special type of heat exchangers which change solar radiation energy to internal energy of the intermediary. Solar collector is an equipment that absorbs the incoming solar radiation, converts into heat and transfers this heat to a fluid (usually water, oil and refrigerant) flow past the collector. The solar energy is collected from the circulating fluid directly to the hot water or space conditioning equipment, or to a thermal energy storage tank from which can be used at night or cloudy days.

In this section an exhibit of the various types of collectors currently available will be presented. This includes Flat plate collectors (FPC), Evacuated tube collectors (ETC), and Stationary compound parabolic collectors (CPC). (ASHRAE, 1995).

2.2.1 Flat-plate collectors

A flat-plate solar collector is shown in Figure 2. When solar radiation passes through a glass cover and impinges on the blackened absorber surface of high absorptivity, a large portion of this energy is absorbed by the plate and then transferred to the transport medium in the fluid tubes to be carried away for storage or use. The liquid tubes can be welded to the absorbing plate, or they can be an integral part of the plate. (Schweiger, 1997) The liquid tubes are connected at both ends by large diameter header tubes.

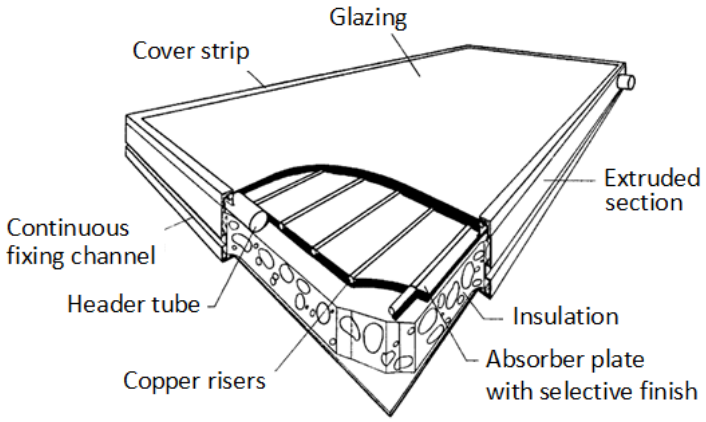

Figure 2.4 Pictorial view of a flat plate collector (source: http://teenet.cmu.ac.th)

The glass cover is used to reduce convection losses from the stagnant air layer between the absorber plate and the glass (Tripanagnostopoulos et al., 2000). It also relieve radiation losses from the collector as the glass to the short wave radiation received by the sun but it is nearly opaque to long-wave thermal radiation emitted by the absorber plate (Wazwaz et al., 2002; Orel et al., 2002). FPC is fixed in position and the optimum tilt angle of the collector is equal to the latitude of the location with angle variations of 10–15 more or less depending on the application.

2.2.2 Compound parabolic collectors

Compound parabolic collectors (CPC) have the exploit of reflecting to the absorber of the solar incident within wide limits. A two parabola trough can be receded moving to absorber the changing solar orientation. (Rabl, 1976; Mills & Giutronich, 1978). CPC can absorb incoming solar radiation over a wide range of angles. By using multiple reflections, the absorber surface located at the bottom of the collector as shown in Figure 2.5 (Tripanagnostopoulos & Yianoulis, 1996).

In Figure 2.5, the lower portion of the reflector is circular, while the upper portions are parabolic. As the upper part of a CPC, the solar radiation is absorbed and truncated thus forming a shorter version of the CPC, which is inexpensive. (Tripanagnostopoulos et al., 1999; Xuesong & Yuezhao, 2004). The concentrator of CPC can be adjusted with a long axis and an aperture is tilted directly towards the equator at an angle equal to the local latitude (McIntire, 1980), the collectors track the sun by turning its axis so as to face the sun continuously.

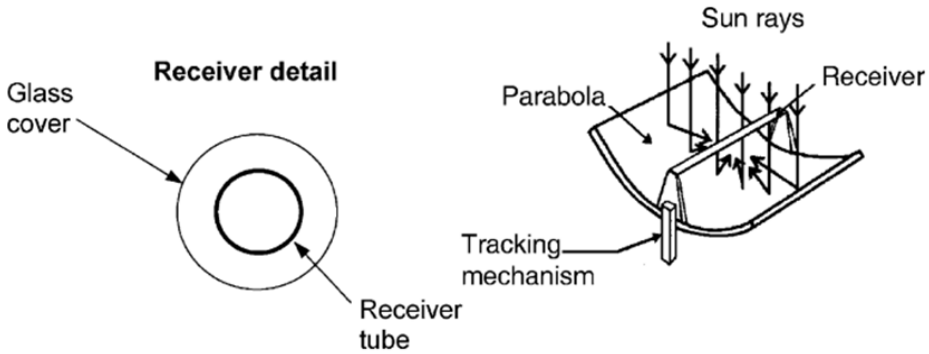

Figure 2.5 Schematic of parabolic trough collector (source: http://teenet.cmu.ac.th)

2.2.3 Evacuated tube collectors

Conventional flat-plate collectors are developed for use in sunny and warm climates. However, the weather conditions impolitic during cold and cloudy days (Nkwetta & Smyth, 2012). Furthermore, influences of weather such as humidity will cause depreciation of internal materials will be affected to performance decrease. Evacuated tube solar collector with heat pipe operates various than the other collectors on the market. ETC consist of a heat pipe inside a vacuum-sealed tube, as shown in Figure 2.6

ETC has presented that the combination of surface selection of coating and an effective convection can result in good performance at high temperatures. The vacuum cover reduces heat convection losses and heat conduction losses, the ETC can operate at higher temperatures than FPC. However, the efficiency of ETC is higher at low tilt angles. This effect tends to give ETC a benefit over FPC in day-long performance (Lin & Furbo, 1998).

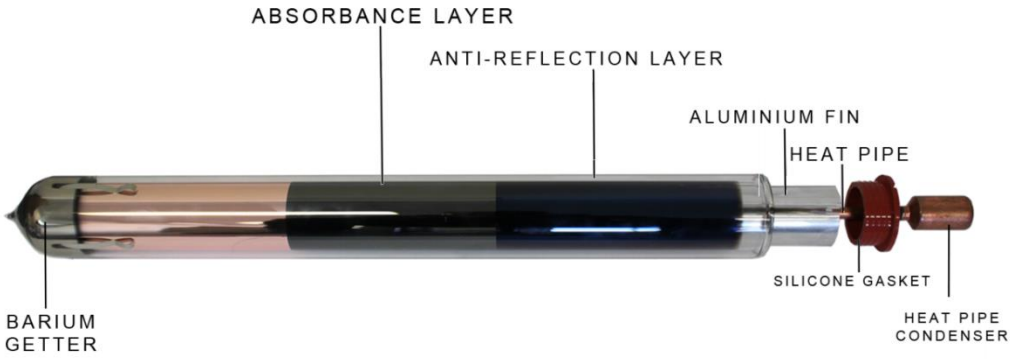

Figure 2.6 Schematic of evacuated glass tube collector
(source: https://en.wikipedia.org/wiki/Solar_thermal_collector)

ETC with heat pipe use the phase change materials of liquid–vapor for transfer heat at high efficiency. The heat pipe is a highly efficient thermal conductor and inserted inside a vacuum-sealed tube. The pipe is a closed copper pipe and mounted to an aluminum fin. The heat pipe filled a small volume of fluid (e.g. water or refrigerant) that can an evaporating-condensing. The evaporating-condensing cycle, solar heat evaporates the liquid, and the vapor moves to the heat sink where it

condenses and removals its latent heat. The condensed fluid return back to the solar collector and the process is repeatedly. The tubes are installed into a heat exchanger (manifold) as shown in Figure 2.7. Water flows pass the manifold and removals the heat from the tubes. The hot water circulates pass the heat exchanger and water is stored in a storage tank.

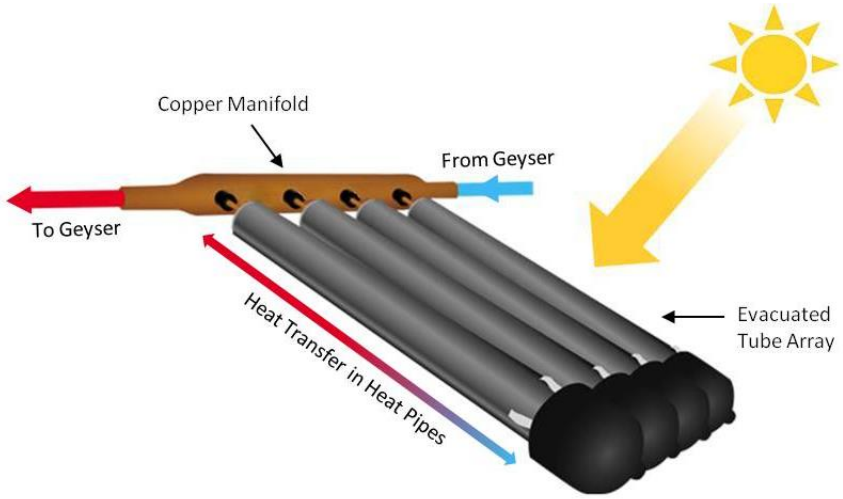

Figure 2.7 Evacuated tube collector system
(source: http://www.solarsense.co.za/solar-water-heating-explained.php)

2.3 Two-phase closed thermosyphon

Two-phase thermosyphon is a gravity-assistee heat pipe. The condenser section is located above the evaporator section so that the condensate is come back by gravity. The operation of the thermosyphon is sensitive to the working fluid fill volume. For thermosyphons, it has been shown experimentally that the heat transfer rate increases with the amount of the working fluid up to a certain value. The capillary limit is the problem of the thermosyphon due to the fact that gravity is the driving force for condensate return (Faghri, 1995).

Heat pipe operating below its maximum overall heat transfer ratethe performance of a heat pipe can be calculated by overall thermal resistance (Z_{tot}). The overall heat transfer rate (Q) and the temperature difference between the heat source and the heat sink (ΔT) are then related by

$$Q = \frac{\Delta T}{Z_{tot}} \tag{2.1}$$

The overall thermal resistance can be represented by idealized network of thermal resistance, Z_1 to Z_{10}, shown in Figure 2.8. The thermal resistance is given in the nomenclature (Zuo and Faghri, 1998).

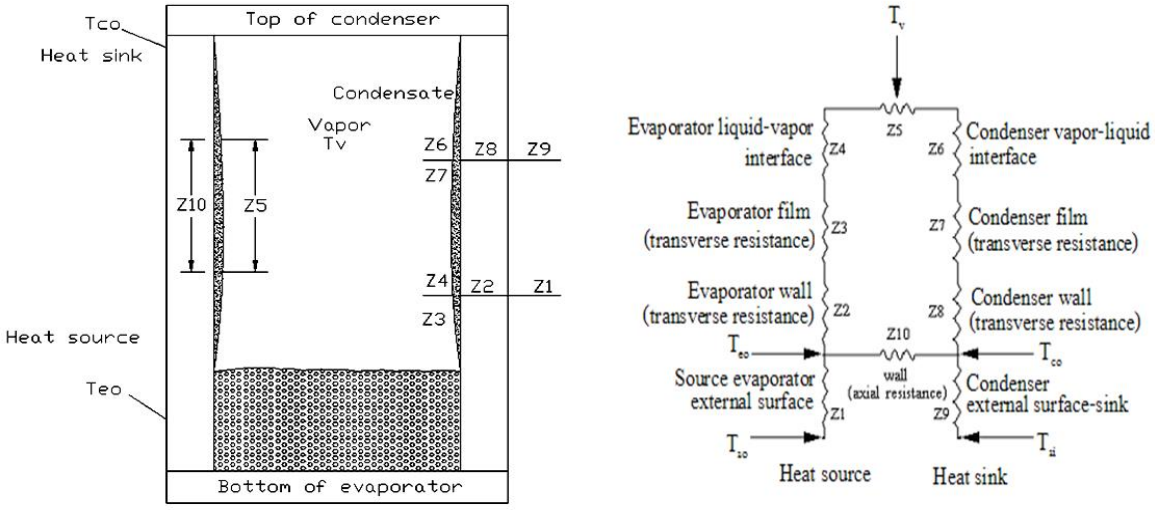

Figure 2.8 Thermal resistance of the thermosyphon (Faghri, 1995)

Z_1 and Z_9 are the thermal resistance between the heat source and the evaporator external surface and between the condenser external surface and the heat sink. In these both of Z_1 and Z_9 can be calculated as

$$Z_1 = \frac{1}{h_e A_e} \tag{2.2}$$

$$Z_9 = \frac{1}{h_c A_c} \tag{2.3}$$

Z_2 and Z_8 are the thermal resistance of wall thickness of the thermosyphon at the evaporator and the condenser, respectively can be calculated as

$$Z_2 = \frac{\ln(D_o / D_i)}{2\pi L_e k} \tag{2.4}$$

$$Z_8 = \frac{\ln(D_o / D_i)}{2\pi L_c k} \tag{2.5}$$

Z_3 and Z_7 are the thermal resistance of film boiling and film condensation in the evaporator and the condenser, respectively

$$Z_3 = Z_{3p}F + Z_{3f}(1-F) \tag{2.6}$$

$$Z_{3f} = \frac{CQ^{1/3}}{D_i^{4/3} g^{1/3} L_e \Phi_2^{4/3}} \tag{2.7}$$

$$Z_{3p} = \frac{1}{\Phi_3 g^{0.2} Q^{0.4} (\pi D_{in} L_e)^{0.6}} \tag{2.8}$$

if $Z_{3p} < Z_{3f}$ define $Z_3 = Z_{3p}$

$$Z_7 = \frac{CQ^{1/3}}{D_{in}^{4/3} g^{1/3} h (\Phi_2)^{4/3}} \tag{2.9}$$

Where Re_f>1300 can be calculated from $Re_f = \frac{4Q}{h\mu\pi D_i}$

$$Z_7 = \frac{CQ^{1/3}}{D_{in}^{4/3} g^{1/3} h_{fg} (\Phi_2)^{4/3}} \; x \; 191 Re_f^{-0.733} \tag{2.10}$$

$$\Phi_2 = \left(\frac{h_{fg} k_f^3 \rho_f^2}{\mu_f}\right)^{0.25} \tag{2.11}$$

Where Φ_2 is merit number (kg/($K^{0.75}S^{2.5}$), C is $\left(\frac{1}{4}\right)\left(\frac{3}{\pi}\right)^{4/3} = 0.235$, Φ_3 can be described by calculating for boiling as provided by Imura et al.(1977).

$$\Phi_3 = 0.32 \frac{\rho_f^{0.65} k_f^{0.3} c_{p_f}^{0.7}}{\rho_v^{0.25} h_{fg}^{0.4} \mu_f^{0.1}} \left[\frac{P_v}{P_a}\right]^{0.23} \tag{2.12}$$

Z_4 and Z_6 are the thermal resistance occurs at the vapor-liquid interfaces of the evaporator and the condenser, respectively.

Z_5 is the effective thermal resistance of the vapor.

Z_{10} is the thermal resistance along the axial length of the thermosyphon wall can be calculated as

$$Z_{10} = \frac{(0.5L_e + L_a + 0.5L_c)}{A_x k} \tag{2.13}$$

Where $A_x = \frac{\pi}{4}(D_o^2 - D_i^2)$

In most practical thermasyphon, axial conduction in the thermasyphon wall is negligible compared to the heat transported by vapor. A practical criterion for negligible axial conduction is

$$\frac{Z_{10}}{Z_2 + Z_3 + Z_4 + Z_5 + Z_6 + Z_7 + Z_8} > 20 \tag{2.14}$$

If Equation (2.13) is satisfied, the overall thermal resistance is

$$Z_{tot} = Z_1 + Z_2 + Z_3 + Z_4 + Z_5 + Z_6 + Z_7 + Z_8 + Z_9 \tag{2.15}$$

But, if Equation (2.14) is not satisfied, the overall thermal resistance is

$$Z_{tot} = Z_1 + [(Z_2 + Z_3 + + Z_4 + Z_5 + Z_6 + Z_7 + Z_8)^{-1} + 1/Z_{10}]^{-1} + Z_9 \tag{2.16}$$

2.4 Heat transfer

2.4.1 Free convection on the long horizontal

In the sections, is considered free convection with laminar boundary and transition of the laminar flow change to a turbulent state. Grashof number (*Gr*) and the Rayleigh number (*Ra*), which presented in empirical correlations of free convection both laminar and turbulent flow conditions. The geometry has been studied extensively, Morgan has been reviewing much existing correlation for an isothermal cylinder as shown in Figure 2.9, Morgan expressed the form:

$$Nu_D = \frac{h_D D}{k} = CRa_D^n \tag{2.17}$$

Where the Rayleigh number,

$$Ra_D = Gr_D\, Pr = \frac{g\beta D^3 (T_s - T_\infty)}{\nu\alpha} \tag{2.18}$$

Where C and n are shown in Table 2.1 and Ra_D and Nu_D are based on the cylinder diameter. In the other hand, Churchill and Chu have introduced a single correlation for a wide Rayleigh number range:

$$Nu_m = h_m \frac{D}{k} = \left\{ 0.60 + \frac{0.387 Ra_D^{1/6}}{\left[1 + \left(\frac{0.559}{\mathrm{Pr}} \right)^{9/16} \right]^{8/27}} \right\}^2 \qquad Ra_D \leq 10^{12} \tag{2.19}$$

Table 2.1 Constant parameters for free convection on a horizontal circular cylinder for Equation 2.16 (Holman, 1989)

$\mathbf{Ra_D}$	**C**	**n**
10^{-10} to 10^{-2}	0.675	0.058
10^{-2} to 10^{2}	1.02	0.148
10^{2} to 10^{4}	0.850	0.188
10^{4} to 10^{7}	0.480	0.250
10^{7} to 10^{12}	0.125	0.333

The above correlations are given the average Nusselt number at the circumference of the cylinder. As shown in Figure 2.9, for the heat of cylinder, Nusselt numbers are ascend by boundary layer development. This decay is dispersed at Rayleigh numbers adequately large ($Ra_D \geq 10^9$) to allow transition to turbulence inside the boundary layer. If the cylinder is cooled relative to the ambient fluid, boundary layer development at $\theta = \pi$, the Nusselt number is a maximum at this location, and the plume descends from the cylinder (Holman, 1989).

The effects of free convection clearly count on the extension coefficient β. The feature in that β is obtained count on the fluid. For an ideal gas, $\rho = p/RT$ and

$$\beta = -\frac{1}{\rho}\left(\frac{\partial p}{\partial T}\right) = \frac{1}{\rho}\frac{p}{RT^2} = \frac{1}{T} \tag{2.20}$$

Note that the properties are calculated at the film temperature, $T = (T_s + T_\infty)/2$.

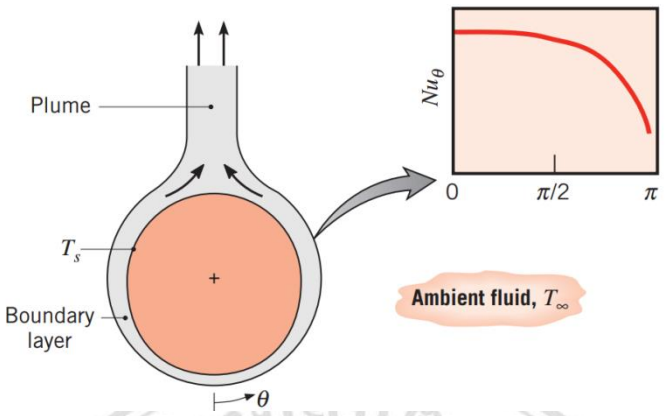

Figure 2.9 Boundary layer and Nusselt number on a horizontal cylinder

2.4.2 Flow across cylinder

Cross flow over a cylinder shows complicated flow patterns as shown in Figure 2.10, the fluid nearly the cylinder ramification out and encircles the cylinder, forming a boundary layer that wraps around the cylinder. The fluid particles on the mid-plane beat the cylinder at the stagnation point, the fluid is a stop and increasing the pressure at that point. The germination of boundary layer transition, which depends on the Reynolds number, strongly influences the position of the separation point. For the round cylinder the characteristic length is the diameter, and the Reynolds number is defined as

$$Re_d = \frac{\rho V D}{\mu} \tag{2.21}$$

Where V is the fluid velocity over the tube and D is the tube diameter.

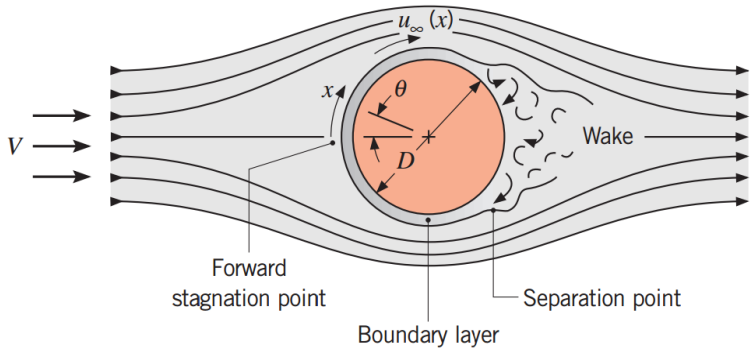

Figure 2.10 Flow cross Flow cylinder

Flows across cylinders, relate to flow separation, which is intricate to analytically. Therefore, flows must be studied experimentally or numerically. Indeed, flow across cylinders has been studied experimentally by several investigators, and several empirical correlations are developed the heat transfer coefficient.

The variation of the Nusselt number (*Nu*) around the circumference of a cylinder. However, the heat transfer calculations require the heat transfer coefficient over the entire surface. The several such relations obtainable in the literature for the Nusselt number of cross flow over a cylinder, the one proposed by Churchill and Bernstein**:**

$$Nu_d = \frac{h_d D}{k} = 0.3 + \frac{0.62\,Re^{1/2}\,Pr^{1/3}}{\left[1+\left(\frac{0.4}{Pr}\right)^{2/3}\right]^{1/4}}\left[1+\left(\frac{Re}{282{,}000}\right)^{5/8}\right]^{4/5} \tag{2.22}$$

Table 2.2 Constant parameters for cross flow cylinder (Cengel, 2004)

$\mathbf{Re_d}$	**A**	**n**
0.4 – 4	0.989	0.33
4 – 40	0.911	0.385
40 – 4000	0.683	0.466
4000 – 40,000	0.193	0.618
40,000 – 400,000	0.0266	0.805

This relation is comprehensive for *Re* (*Pr>0.2*). The fluid properties are evaluated at the film temperature, which is the average of the free-stream and surface temperatures. The Nusselt number of flow across cylinders can be expressed as:

$$Nu_d = \frac{h_d D}{k} = (A)(Re_d)^n (Pr)^{1/3} \tag{2.23}$$

Where the constants *A* and *n* are shown in Table 2.2

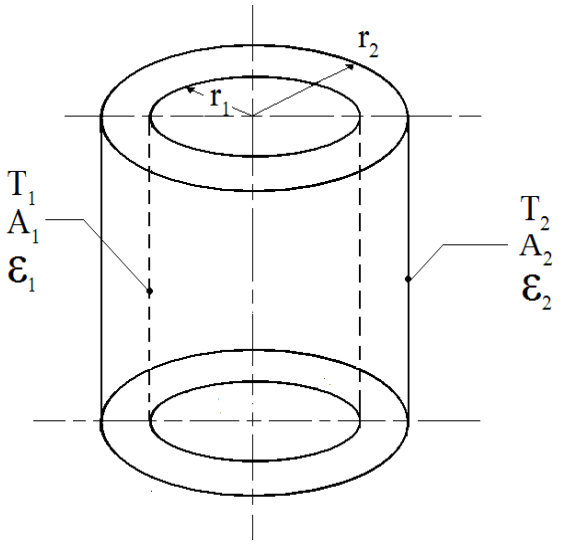

Figure 2.11 Radiation between two concentric cylinders

2.4.3 Radiation heat transfer in two-surface enclosures

Consider a radiation between these infinitely long concentric cylinders as shown in Figure 2.11. Surfaces 1 and 2 have emissivity ε_1 and ε_2, surface areas A_1 and A_2 and uniform temperatures T_1 and T_2, respectively. That is, the radiation rate of heat transfer from surface 1 to surface 2 is equal to the radiation rate of heat transfer from surface 1 and the radiation rate of heat transfer to surface 2, uniform temperatures T_1 and T_2 (Cengel, 2004) is given by

$$Q_{1\to 2.net} = \frac{\sigma A_1 (T_1^4 - T_2^4)}{\frac{1}{\varepsilon_1} + \frac{r_1}{r_2}\left(\frac{1-\varepsilon_2}{\varepsilon_2}\right)} \tag{2.24}$$

2.5 Performance of evacuated tube solar collectors

The heat transfer rate of the water at a storage tank can be calculated by the different water temperature, taking into the mass of water and its specific heat (Mehmet & Hikmet, 2005).

$$Q_{useful} = m_w c_{p,w}(T_{w2} - T_{w1}) \tag{2.25}$$

Where m_w is the mass of water at a storage tank (kg), $c_{p,w}$ is the specific heat of water (kJ/kg-C), T_{w1} is the temperature of the water at start of the day while T_{w2} is the water temperature at the actual time. The solar energy incident on the surface is given by,

$$Q_{incident} = A\int_{1}^{2} I_G(\tau\alpha)dt \tag{2.26}$$

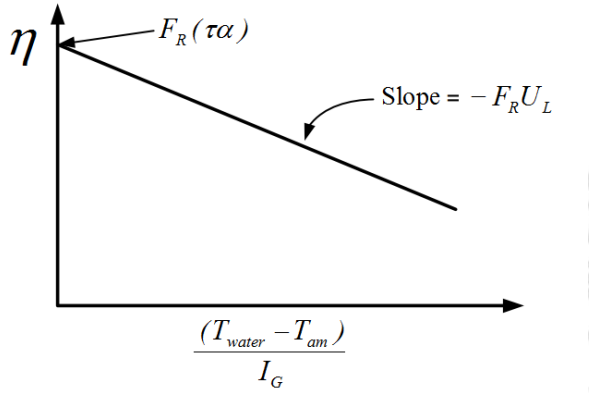

Figure 2.12 Thermal efficiency of solar collector

Where A is the area of surface (m^2), I_G is the solar irradiance (W/m^2). Heat transfer rate of solar collector ($Q_{collector}$) is given by

$$Q_{uesful} = AF_R[I_G(\tau\alpha) - U_L(T_{water} - T_{am})] \tag{2.27}$$

Where F_R is the heat removal factor influenced by the heat transfer resistance between the heated absorber surface and the collector fluid and U_L is the heat loss coefficient. Thus, Equation (2.26) is Hottel-Whillier-Bliss's correlation.

The collector efficiency (η) can be calculated as a ratio of heat stored in water to the total solar energy incident on the surface is given by,

$$\eta = \frac{Q_{useful}}{Q_{incident}} \tag{2.28}$$

From Equation (2.26) and (2.27), the efficiency of solar collector is explained that it can convert the solar irradiation to heat energy (Vorayos et al., 2009). The formula is as follow.

$$\eta = \frac{Q_{useful}}{I_G A} = F_R(\tau\alpha) - \frac{F_R U_L (T_{water} - T_{am})}{I_G} \quad (2.29)$$

Moreover, the correlation between $(T_{water} - T_{am})/I_G$ and thermal efficiency from Equation (2.29) are plotted in Figure 2.12.

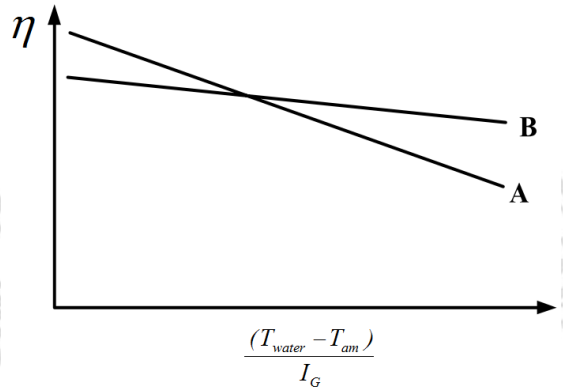

Figure 2.13 Comparisons solar collector efficiency

Where $F_R U_L$ represents the heat loss coefficient. Due to high value, the solar collector has poor thermal protection. So, both solar collector A and B are compared to the thermal efficiency as shown in Figure 2.13. It should be noted that the A collector can be used appropriately at low temperature while the B collector can be used appropriately at high temperature.

2.6 Finite difference

There are several ways of the numerical formulation of a heat conduction problem, such as the finite difference method, the finite element method, the boundary element method, and the energy balance (or control volume) method. Each method has its own good point and bad point. The numerical methods for calculating differential equations are based on Taylor's series expanded about point (*i* ,*j*) as follows

$$u_{i+1,j} = u_{i,j} + \left(\frac{\partial u}{\partial x}\right)_{i,j} (\Delta x) + \left(\frac{\partial^2 u}{\partial x^2}\right)_{i,j} \frac{(\Delta x)^2}{2} + \left(\frac{\partial^3 u}{\partial x^3}\right)_{i,j} \frac{(\Delta x)^3}{6} + \ldots \quad (2.30)$$

Solving $(\partial u/\partial x)_{i,j}$ from Equation (2.29), is obtained

$$\left(\frac{\partial u}{\partial x}\right)_{i,j} = \left(\frac{u_{i+1,j} - u_{i,j}}{\Delta x}\right) - \left(\frac{\partial^2 u}{\partial x^2}\right)_{i,j} \frac{(\Delta x)^2}{2} - \left(\frac{\partial^3 u}{\partial x^3}\right)_{i,j} \frac{(\Delta x)^3}{6} - \ldots \tag{2.31}$$

In Equation (2.31), the derivative evaluated at point (*i, j*) is given on the left side. The first term on the right side, is a finite difference description of the partial derivative. The remaining terms on the right side composed of the truncation error. That is, the approximate the partial derivative with the algebraic finite difference,

$$\left(\frac{\partial u}{\partial x}\right)_{i,j} \approx \left(\frac{u_{i+1,j} - u_{i,j}}{\Delta x}\right)_{i,j} \tag{2.32}$$

The truncation error in Equation (2.32) is neglected in this approximation. In Equation (2.31), the lowest-order term in the truncation error involves Δx to the first power; hence, the finite difference expression in Equation (2.33) is call first order, can write Equation (2.32) as

$$\left(\frac{\partial u}{\partial x}\right)_{i,j} = \left(\frac{u_{i+1,j} - u_{i,j}}{\Delta x}\right) + O(\Delta x) \tag{2.33}$$

In Equation (2.33), the $O\Delta x$ is a symbol mathematical which represents "terms of order".

In Equation (2.33) uses information to right of grid point (*i,j*), that is, $u_{i+1,j}$ and $u_{i,j}$. No information to the left of (*i,j*) is used. Therefore, the first order difference explanation for the derivative $(\partial u/\partial x)_{i,j}$ expressed by Equation (2.33) as a first order difference. Taylor series expansion for $u_{i-1,j}$ expanded about $u_{i,j}$.

$$u_{i-1,j} = u_{i,j} + \left(\frac{\partial u}{\partial x}\right)_{i,j} (-\Delta x) + \left(\frac{\partial^2 u}{\partial x^2}\right)_{i,j} \frac{(-\Delta x)^2}{2} + \left(\frac{\partial^3 u}{\partial x^3}\right)_{i,j} \frac{(-\Delta x)^3}{6} + \ldots \tag{2.34}$$

Solving for $(\partial u/\partial x)_{i,j}$, is obtained

$$\left(\frac{\partial u}{\partial x}\right)_{i,j} = \left(\frac{u_{i,j} - u_{i-1,j}}{\Delta x}\right) + O(\Delta x) \tag{2.35}$$

The information used in the finite difference quotient in Equation (2.35) comes from the left of grid point (*i,j*) ; that is, it uses $u_{i-1,j}$ and $u_{i,j}$. As a result, the finite difference in Equation (2.35) is call a rearward or backward difference.

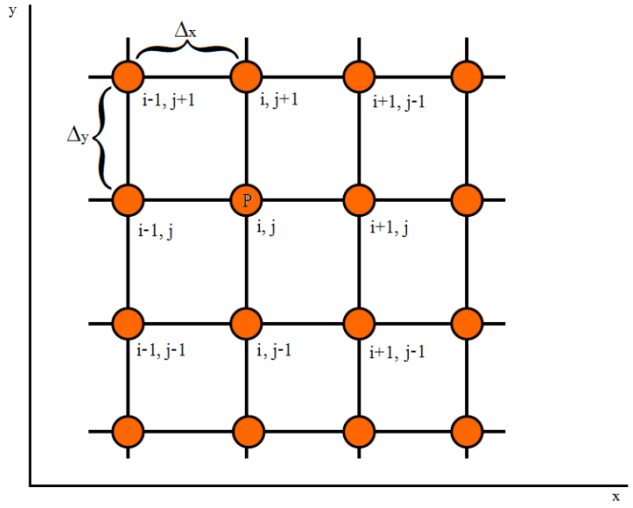

Figure 2.14 Discrete grid point (Holman, 1989)

In most applications in CFD, first-order accuracy is not sufficient. To construct a finite difference of second-order accuracy as

$$u_{i+i,j} - u_{i-1,j} = 2\left(\frac{\partial u}{\partial x}\right)_{i,j}(\Delta x) + 2\left(\frac{\partial^3 u}{\partial x^3}\right)_{i,j}\frac{(\Delta x)^3}{6} + \ldots \tag{2.36}$$

Equation (2.36) can be written as

$$\left(\frac{\partial u}{\partial x}\right)_{i,j} = \frac{u_{i+1,j} - u_{i-1,j}}{2\Delta x} + O(\Delta x)^2 \tag{2.37}$$

The information used in the finite difference quotient in Equation (2.37) comes from both side of the grid point located at (*i,j*) ; that is, it uses $u_{i+1,j}$ to $u_{i-1,j}$. Grid point (*i,j*) falls between the two nearby grid points. The finite difference in Equation (2.37) is calling a second order central difference. The results are analogous to the previous equation for the x derivative. They are:

$$\left(\frac{\partial u}{\partial y}\right)_{i,j} = \begin{cases} \dfrac{u_{i,j+1} - u_{i,j}}{\Delta y} + O(\Delta y) & \text{Forward difference} \quad (2.38) \\ \dfrac{u_{i,j} - u_{i,j-1}}{\Delta y} + O(\Delta y) & \text{Backward difference} \quad (2.39) \\ \dfrac{u_{i,j+1} - u_{i,j-1}}{2\Delta y} + O(\Delta y)^2 & \text{Central difference} \quad (2.40) \end{cases}$$

Consequently, there is a need for second-order derivatives of CFD. We can obtain such finite difference expressions by continuing with a Taylor series analysis, as follows.

$$u_{i+1,j} + u_{i-1,j} = 2u_{i,j} + \left(\frac{\partial^2 u}{\partial x^2}\right)_{i,j} (\Delta x)^2 + \left(\frac{\partial^4 u}{\partial x^4}\right)_{i,j} \frac{-\Delta x^4}{12} + \ldots \quad (2.41)$$

Solving $(\partial^2 u / \partial x)_{i,j}$,

$$\left(\frac{\partial^2 u}{\partial x^2}\right)_{i,j} = \frac{u_{i+1,j} - 2u_{i,j} + u_{i-1,j}}{(\Delta x)^2} + O(\Delta x)^2 \quad (2.42)$$

In Equation (2.42), the first term on right-hand side is a central finite difference for the second derivative with respect to x evaluated at grid point (*i,j*). An expression can easily be obtained for the second derivative of y-axis, with the result that

$$\left(\frac{\partial^2 u}{\partial y^2}\right)_{i,j} = \frac{u_{i+1,j} - 2u_{i,j} + u_{i-1,j}}{(\Delta y)^2} + O(\Delta y)^2 \quad (2.43)$$

Equation (2.41) and (2.42) are examples of second-order central second difference. Many other difference approximations can be obtained for the same derivative above, as show in Figure 2.15.

2.6.1 Difference equation

When all the partial derivatives in a partial differential equation are replaced by finite difference, the resulting algebraic equation is called a difference equation, which is an algebraic representation of the partial differential equation. The finite difference solutions in CFD is to use the difference derived to replace the partial

derivatives in the governing flow equation, resulting in a system of algebraic difference equations for the dependent variables at each grid point. One-dimensional heat conduction equation with constant thermal diffusivity, repeated below

$$\frac{\partial T}{\partial t} = \alpha \frac{\partial^2 T}{\partial x^2} \tag{2.44}$$

The partial derivative in Equation (2.44) with finite difference. Equation (2.44) has two variables, *x* and *t*. Here, *i* is the index in the *x*-axis and *n* is the index in the *t*-axis. For example, instead of the time derivatives in Equation (2.44) with central difference patterned after Equation (2.42).

$$\left(\frac{\partial^2 T}{\partial x^2}\right)_i^n = \left(\frac{T_{i+1}^n - 2T_i^n + T_{i-1}^n}{\Delta x^2}\right) - \left(\frac{\partial^4 T}{\partial x^4}\right)_i^n \frac{\Delta x^2}{2} + \ldots \tag{2.45}$$

Writing just the difference equation from Equation (2.45) as

$$\left(\frac{T_i^{n+1} - T_i^n}{\Delta t}\right) = \alpha\left(\frac{T_{i+1}^n - 2T_i^n + T_{i-1}^n}{\Delta x^2}\right) \tag{2.46}$$

Equation (2.46) is a difference equation which indicated the original partial difference equation expressed in Equation (2.44), However, Equation (2.46) is just an approximation.

First-order

Backward difference $\left(\frac{\partial u}{\partial y}\right)_{i,j} = \left(\frac{u_{i,j} - u_{i,j-1}}{\Delta y}\right)$

with respect to y

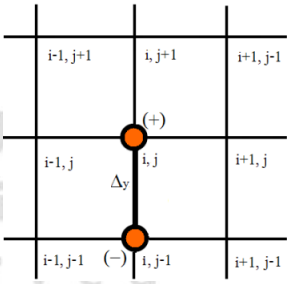

Second-order

Central difference $\left(\frac{\partial u}{\partial y}\right)_{i,j} = \left(\frac{u_{i,j+1} - u_{i,j-1}}{2(\Delta y)}\right)$

with respect to y

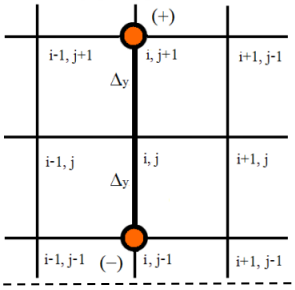

Figure 2.15 Finite difference expressions with their appropriate finite difference modules (Holman, 1989)

First-order

Forward difference $\left(\frac{\partial u}{\partial x}\right)_{i,j} = \left(\frac{u_{i+1,j} - u_{i,j}}{\Delta x}\right)$

with respect to x

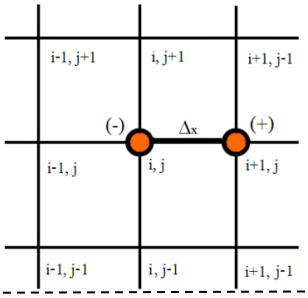

First-order

Backward difference $\left(\frac{\partial u}{\partial x}\right)_{i,j} = \left(\frac{u_{i+1,j} - u_{i,j}}{\Delta x}\right)$

with respect to x

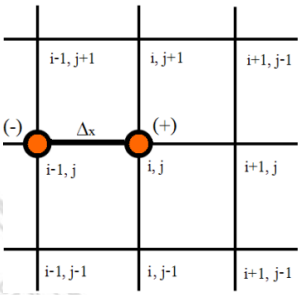

Second-order

Central difference $\left(\frac{\partial u}{\partial x}\right)_{i,j} = \left(\frac{u_{i+1,j} - u_{i-1,j}}{2(\Delta x)}\right)$

with respect to x

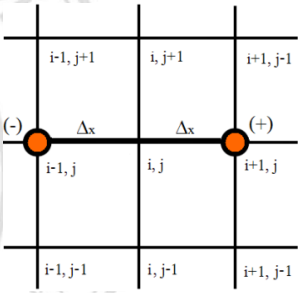

Second-order

Central second difference $\left(\frac{\partial^2 u}{\partial x^2}\right)_{i,j} = \left(\frac{u_{i+1,j} - 2u_{i,j} + u_{i-1,j}}{(\Delta x)^2}\right)$

with respect to x

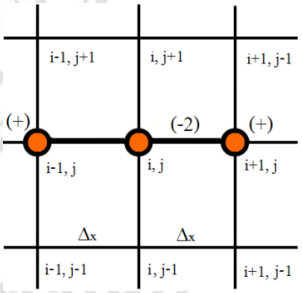

First-order

Forward difference $\left(\frac{\partial u}{\partial y}\right)_{i,j} = \left(\frac{u_{i,j+1} - u_{i,j}}{\Delta y}\right)$

with respect to y

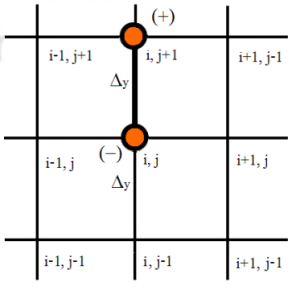

Figure 2.15 Finite difference expressions with their appropriate finite difference modules (Holman, 1989)

2.6.2 Explicit and Implicit Finite Difference Method

Aspects of several difference techniques commonly used in CFD. However, the specific technique of solve a problem, an explicit approach or an implicit approach are presented. It is suitable to define these two general approaches. Explicit and implicit approaches are using for model equation without the complexity of the governing equation. $\partial T/\partial t$ is a forward difference and $\partial^2 T/\partial x^2$ is a central second difference, leading to the form of the difference equation given by Equation (2.46), this equation can be written as

$$T_i^{n+1} = T_i^n + \alpha\left(\frac{\Delta t}{\Delta x^2}\right)(T_{i+1}^n - 2T_i^n + T_{i-1}^n) \tag{2.47}$$

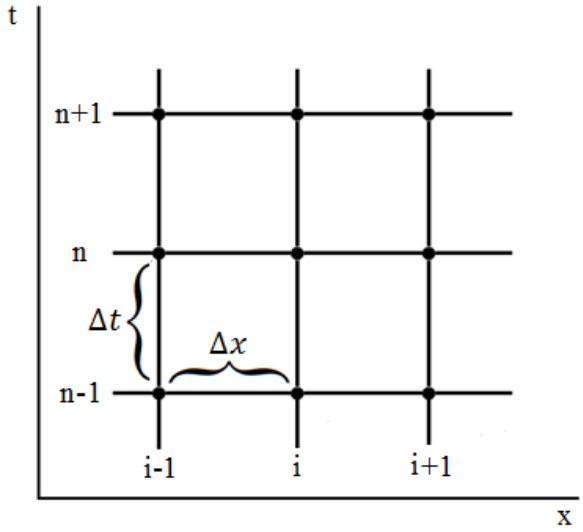

Figure 2.16 Grid for the differencing of Equation (2.43) (John & Anderson, 2005)

The variable here is time *t*. To specific, consider the finite difference grid in Figure 2.17. Assume *T* is known at all grid point at time *t* level *n*. Time means that *T* at all grid point at time level *n + 1* are calculated from known values at time level *n*. When this calculated is finished, we have known values at time level *n + 1*. Then the same procedure is used calculated *T* at all grid point at time level *n + 2*, using the known values at level *n + 1*. The solution is progressively obtained in steps of time. Equation (2.46) is written with properties at time level *n* on the right-hand side and properties at time level *n + 1* on the left-hand side, all properties at level *n* are known and those at level *n + 1* are to be calculated. The particular significance is that only one

known shown in Equation (2.46), namely, T_i^{n+1}. Hence, Equation (2.46) allows for the immediate solution of T_i^{n+1} from the known properties at time level *n*. We have a single equation with a single unknown. For example, consider the grid shown in Figure 2.18, where the distribution of seven grid points along the x-axis. Centering on grid point 2, Equation (2.47) is written as

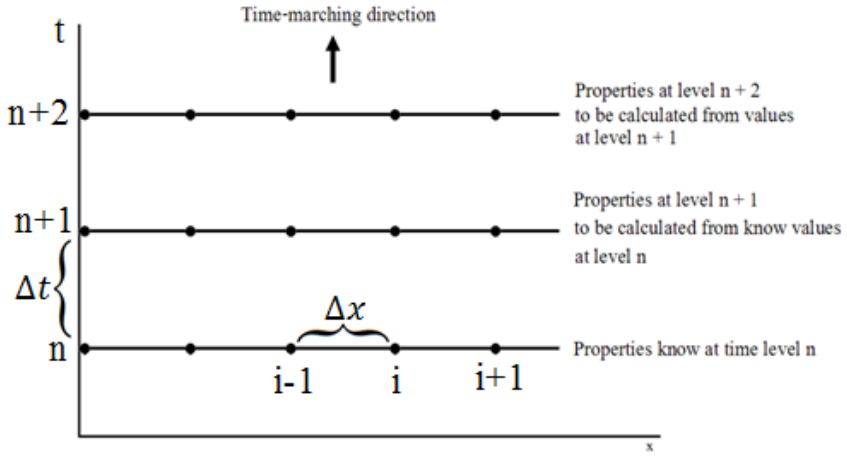

Figure 2.17 Illustration of time marching (John & Anderson, 2005)

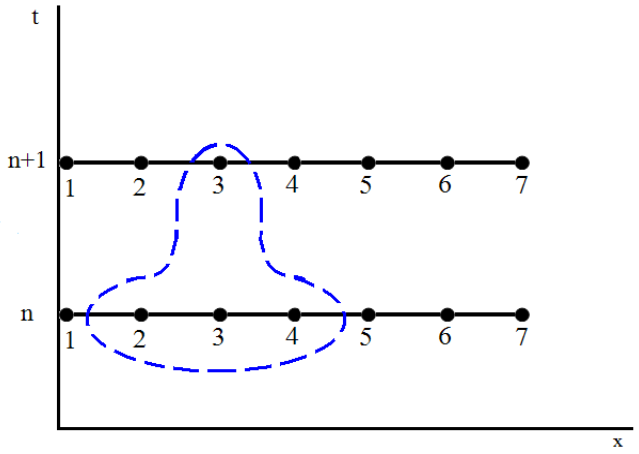

Figure 2.18 Explicit finite difference modules (John & Anderson, 2005)

$$T_2^{n+1} = T_2^n + \alpha\left(\frac{\Delta t}{\Delta x^2}\right)(T_3^n - 2T_2^n + T_1^n) \tag{2.48}$$

An explicit approach of difference equation has one unknown and can be solved explicit for this unknown in a straightforward manner. This explicit approach is further illustrated by the finite difference module constrained within the dashed balloon in Figure 2.18. Here, the module contains only one unknown at time level *n+1*. In Equation (2.44), this time writing the spatial difference on the right-hand side in terms of average properties between time levels *n* and *n +1*, will represent by

$$\frac{T_i^{n+1}-T_i^n}{\Delta t}=\alpha\left(\frac{\frac{1}{2}(T_{i+1}^{n+1}+T_{i+1}^n)+\frac{1}{2}(-2T_i^{n+1}-2T_i^n)+\frac{1}{2}(T_{i-1}^{n+1}+T_{i-1}^n)}{\Delta x^2}\right) \tag{2.49}$$

The differencing in Equation (2.49) is called the Crank-Nicolson. The unknown T_i^{n+1} is not only shown in terms of the known at time level *n*. namely, T_{i+1}^n, T_i^n and T_{i-1}^n, but in terms of other unknown at time level *n + 1*, namely, T_{i+1}^{n+1} and T_{i-1}^{n+1}. Equation (2.49) represents one equation with three unknown, namely, T_{i+1}^{n+1}, T_i^{n+1} and T_{i-1}^{n+1}.

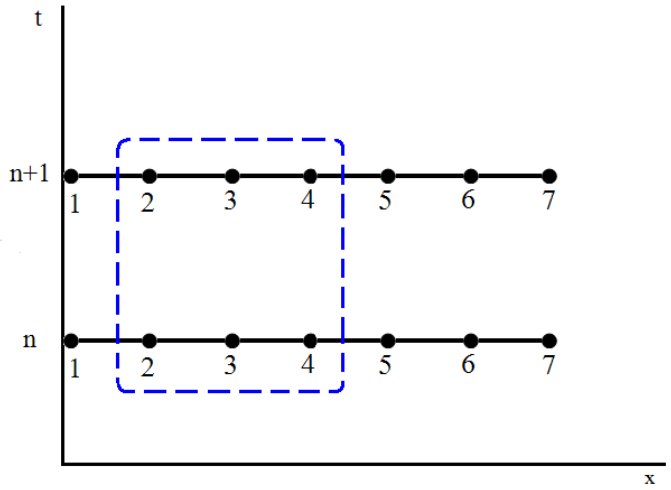

Figure 2.19 Implicit finite difference modules (John & Anderson, 2005)

Equation (2.48) can be rearranged to the unknowns on the left-hand side and the known number on the right-hand side. The result is

$$\frac{\alpha\Delta t}{2(\Delta x)^2}T_{i-1}^{n+1}-\left[1+\frac{\alpha\Delta t}{(\Delta x)^2}\right]T_i^{n+1}+\frac{\alpha\Delta t}{2(\Delta x)^2}T_{i+1}^{n+1}=-T_i^n-\frac{\alpha\Delta t}{2(\Delta t)^2}(T_{i+1}^n-2T_i^n+{}_{i-1}^n) \quad (2.50)$$

Simplifying the nomenclature by denoting the following by *A*, *B*, and *Ki*

$$A=\frac{\alpha\Delta t}{2(\Delta x)^2},\ B=\left[1+\frac{\alpha\Delta t}{(\Delta x)^2}\right],\ K_i=-T_i^n-\frac{\alpha\Delta t}{2(\Delta t)^2}(T_{i+1}^n-2T_i^n+{}_{i-1}^n)$$

Write Equation (2.50) in the form

$$AT_{i-1}^{n+1}-BT_i^{n+1}+AT_{i+1}^{n+1}=K_i \quad (2.51)$$

Note that *Ki* in Equation (2.51) consists of propertied at time level *n*, which are known. Hence, *Ki* is a known number in Equation (2.51). Returning to Figure 2.19, we now apply Equation (2.51) sequentially to grid point 2 through 6

At grid point 2 $$AT_1-BT_2+AT_3=K_2 \quad (2.52)$$

Hence, in Equation (2.52) the term involving the known T_1 can be transferred to the right-hand side and denoting K_2 - AT_1 by K_2', where K_2' is a known number, Equation (2.52) is written as

$$-\mathrm{BT}_2+\mathrm{AT}_3=\mathrm{K}_2' \quad (2.53)$$

At grid point 3 $$AT_2-BT_3+AT_4=K_3 \quad (2.54)$$

At grid point 4 $$AT_3-BT_4+AT_5=K_4 \quad (2.55)$$

At grid point 5 $$AT_4-BT_5+AT_6=K_5 \quad (2.56)$$

At grid point 6 $$AT_5-BT_6+AT_7=K_6 \quad (2.57)$$

In Equation (2.57), since grid point 7 is on a boundary, T_7 is known from the defined boundary condition. Hence, Equation (2.58) can be rearranged as

$$AT_5-BT_6=K_6-AT_7=K_6' \quad (2.58)$$

Where K_6' is a known number. Equations (2.51) to (2.55) are five equations for the five unknowns T_2, T_3, T_4, T_5 and T_6. This system of equation can be written in matrix form as follows.

$$\begin{bmatrix} -B & A & 0 & 0 & 0 \\ A & -B & A & 0 & 0 \\ 0 & A & -B & A & 0 \\ 0 & 0 & A & -B & A \\ 0 & 0 & 0 & A & -B \end{bmatrix} \begin{bmatrix} T_2 \\ T_3 \\ T_4 \\ T_5 \\ T_6 \end{bmatrix} = \begin{bmatrix} K_2' \\ K_3 \\ K_4 \\ K_5 \\ K_6' \end{bmatrix} \tag{2.59}$$

The coefficient matrix is a tri-diagonal matrix. The system solved by Equation (2.58) involves the formulation of the tri-diagonal arrangement; such solutions are usually obtained using "Thomas' algorithm" (John & Anderson, 2005).

2.6.3. The Explicit Method of cylinder coordinates

Transient conduction of long cylinders is considered in this section. From one-dimensional heat conduction equation in Equation (2.44) is modified for a long cylinder. The conduction equation for the instantaneous temperature rise T (r, θ, z, t), the temperature (T_i) in the region of a long circular cylinder as follows:

$$\frac{1}{\alpha}\frac{\partial T}{\partial t} = \frac{\partial^2 T}{\partial r^2} + \frac{1}{r}\frac{\partial T}{\partial r} + \frac{1}{r^2}\frac{\partial^2 T}{\partial \theta^2} + \frac{\partial^2 T}{z^2} + \frac{\dot{q}}{k} \tag{2.60}$$

Where α is thermal diffusivity ($k/\rho C_p$)

The partial derivative in Equation (2.60) with finite difference. Equation (2.60) has four variables, x θ, z, and t. Here, r is the index in the r-direction, θ is the index in the θ-direction, z is the index in the z-direction, and n is the index in the time. For example, instead of the time derivatives in Equation (2.60) with central difference patterned as follows:

$$\frac{T^{n}_{(r,\theta,z)} - T^{n-1}_{(r,\theta,z)}}{\alpha \Delta t} = \frac{T^{n-1}_{(r+1,\theta,z)} - 2T^{n-1}_{(r,\theta,z)} + T^{n-1}_{(r-1,\theta,z)}}{\Delta r^{2}} + \frac{1}{\Delta r}\frac{T^{n-1}_{(r+1,\theta,z)} - T^{n-1}_{(r-1,\theta,z)}}{2\Delta r} + \frac{1}{(\Delta r)^{2}}\frac{T^{n-1}_{(r,\theta+1,z)} - 2T^{n-1}_{(r,\theta,z)} + T^{n-1}_{(r,\theta-1,z)}}{\Delta \theta^{2}} + \frac{T^{n-1}_{(r,\theta,z+1)} - 2T^{n-1}_{(r,\theta,z)} + T^{n-1}_{(r,\theta,z-1)}}{\Delta z^{2}} + \frac{\dot{q}}{k} \tag{2.61}$$

2.7 Economic analysis

2.7.1 The payback period

Payback period is the time in which the initial cash outflow of an investment is expected to be recovered from the cash inflows generated by the investment. The formula to calculate payback period is:

$$Payback\ Period = \frac{Initial\ Investment}{Cash\ Inflow\ per\ Period} \tag{2.62}$$

In a case of cash, inflows are discontinuous use the formula for payback period as:

$$Payback\ Period = \mathrm{A} + \frac{B}{C} \tag{2.63}$$

In the above formula,

A is the last period with a negative cash flow

B is the absolute value of cash flow at the end of the period A

C is the total cash flow during the period after A

2.7.2 Return on investment (ROI)

ROI measures the amount of return on an investment relative to the investment's cost. To calculate ROI, the benefit (or return) of an investment is divided by the cost of the investment, and the result is expressed as a percentage or a ratio. The return on investment formula:

$$ROI = \frac{Gain\ from\ Investment - Cost\ of\ Investment}{Cost\ of\ Investemt} \tag{2.64}$$

In the formula, "Gain from Investment" refers to the proceeds obtained from the sale of the investment of interest. Because ROI is measured as a percentage, it can be easily compared with returns from other investments.

2.7.3 Net present value (NPV)

The NPV is used to determine the present value of an investment by the discounted sum of all cash flows received from the project, can be rewritten as

$$NPV = -C_0 + \sum_{t=1}^{T} \frac{C_t}{(1+r)^t} \tag{2.65}$$

Where $-C_0$ is initial investment, C is net cash inflow during the period i, r is discount rate, t is number of time periods. The investment is important to calculate an estimate of profitable the project. In the formula, the $-C_0$ is the initial investment, which is a negative cash flow showing that money is going out as resisted to coming in. The net present value would need to be positive for considered a valuable investment.

2.7.4 Internal rate of return (IRR)

IRR is used in capital measuring the profitability of potential investments. Internal rate of return is a discount rate that makes the NPV of all cash flows from a particular project equal to zero. IRR calculations rely on the same formula as NPV does. To calculate IRR using the formula, one would set NPV equal to zero and solve for the discount rate r. IRR can be calculated through trial-and-error or using programmed to calculate IRR.

2.8 Related statistics

A statistical index is used to validate the model with the experimental data and also used to show the level of an error, generally consists of a coefficient of determination and a normalized root mean squares deviation.

2.8.1 Coefficient of determination (R^2)

R-squared (R^2) is a statistic that explains the amount of variance accounted for in the relationship between two (or more) variables. Sometime R^2 is called the

coefficient of determination, and it is given as the square of a correlation coefficient. This coefficient shows the proportion between the sum of squares for error (*SSE*), sum of squares for the regression (*SSR*) and the total sum of the squares (*SST*). The sum of squared errors (*SSE*), or the sum of squared residuals, is given by

$$SSE = \sum_{i=1}^{n} (y_i - x_i)^2 = \sum_{i=1}^{n} (sim_i - exp_i)^2 \tag{2.66}$$

SSE measures the amount of variability in y_i that is not explained by the model. Then how does one measure the amount of variability in x_i that is explained by the model.

To answer this question, one needs to know the total variability present in the data. The *SST* is the measure of total variation in the *y* variable and is defined as

$$SST = \sum_{i=1}^{n} (y_i - \bar{y})^2 = \sum_{i=1}^{n} (sim_i - \overline{sim})^2 \tag{2.67}$$

Where $\bar{y}$ is the sample mean of y_i variables, that is,

$$\bar{y} = \frac{1}{n} \sum_{i=1}^{n} y_i \tag{2.68}$$

Since *SSE* is the minimum of the sum of squared residuals of any linear model, SSE is always smaller than *SST*. Then the amount of variability explained by the model is *SST* − *SSE*, which is denoted as the regression sum of squares (*SSR*), that is,

$$SSR = \sum_{i=1}^{n} (x_i - \bar{y})^2 = \sum_{i=1}^{n} (exp_i - \overline{sim})^2 \tag{2.69}$$

The ratio *SSR/SST* measures the proportion of variability explained by the model. The coefficient of determination (R^2) is defined as the ratio

$$R^2 = \frac{SSR}{SST} = 1 - \frac{SSE}{SSE} \tag{2.70}$$

Note that the coefficient of determination ranges between 0 and 1. R^2 value is interpreted as the proportion of variation in experimental that is explained by the model.

2.8.2 Standard deviation

The root-mean-square deviation (RMSD) is a frequently used measure of the differences between value predicted by a model and the experimental value. The RMSD represents the sample standard deviation (SD) of the differences between predicted values and experimental values. Both RMSD and SD can be calculated from.

$$RMSD,SD = \sqrt{\frac{1}{N-1}\sum_{i=1}^{N}(y_i - x_i)^2} = \sqrt{\frac{1}{N-1}\sum_{i=1}^{N}(sim_i - exp_i)^2} \quad (2.71)$$

In addition, the percentage of standard deviation (STD) can also be obtained by the normalization of the SD with respect to the mean of the experimental data and multiply by a constant 100. The STD can be obtained from

$$STD = \frac{SD}{\bar{x}} \times 100 \quad (2.72)$$

In this study, STD is used to be a statistical index to validate the model with the experimental data because it can indicate the percentage the deviation of an error between the simulation results and the experimental results by comparing with the experimental data.